Semianalytical Solution for Simultaneous Distribution of Fluid Velocity and Sediment Concentration in Open-Channel Flow

Shiv Mohan[1]; Manotosh Kumbhakar[2]; Koeli Ghoshal[3]; and Jitendra Kumar[4]

Abstract: To understand the sediment-transport process in an open-channel turbulent flow, the time-averaged profiles of streamwise fluid velocity and volumetric particle concentration in suspension must be given simultaneous treatment because they are closely interrelated through particle–turbulence interaction. Presence of sediment particles increases the density of a fluid-sediment mixture, which makes the flow stratified and obstructs the settling of sediment particles. The greater the amount of sediment particles in fluid, the stronger the effects of stratification and hindered settling. Therefore, generalizing existing works, this study attempts to model the velocity and concentration simultaneously, incorporating the aforementioned effects. The coupled system of odes arising from the derivation is strongly nonlinear in nature, and the analytical solution needs a special mathematical tool. To that end, a novel analytical method called the homotopy analysis method (HAM) is employed to obtain the explicit series solution to the system. The methodology is a nonperturbation approach, and the convergence can be tackled easily through some convergence control parameters. The solutions obtained are found to be stable and are validated with numerical solution as well as with relevant experimental data available in the literature. Further, the models have been physically interpreted through the effects of the turbulent factors incorporated. **DOI: 10.1061/(ASCE)EM.1943-7889.0001671.**

Author keywords: Sediment concentration; Fluid velocity; Stratification; Analytical solution; Homotopy analysis method.

Introduction

Problems related to flows carrying suspended sediment are an important topic of research in the field of fluvial hydrodynamics due to their direct practical concern for many engineering applications. For better understanding of the sediment-transport mechanism in a turbulent flow, experimental and theoretical investigations have long been carried out, and numerous models have been developed. But the fluctuating behavior of turbulence always makes its nature unpredictable and does not allow any model to be universal that can be applied under any hydraulic condition. Therefore, investigations on turbulent flow can never come to an end. The streamwise velocity of fluid, as well as the suspended-sediment concentration along a vertical, play significant roles in the erosion and transportation process of sediment. The present study attempts to make a prediction of both the vertical distribution of time-averaged fluid velocity in the streamwise direction and particle concentration in suspension together to gain comprehensive knowledge on the mechanism of sediment transport.

Modeling of the vertical distribution of streamwise velocity and particle concentration started in the twentieth century. Credit for the first development of analytical expressions of velocity and concentration goes to Prandtl (1932) and Rouse (1937), respectively. Rouse (1937) used the logarithmic law of velocity distribution established by Prandtl (1932) and found an analytical solution for the one-dimensional diffusion equation, which is famous under his name (Rouse equation) only. Following their works, researchers continued developing models incorporating several effects such as particle–particle collision, particle–turbulence interaction, secondary current, damping of mixing length, and hindered settling due to presence of particles, among others. Mostly, researchers concentrated either on velocity distribution (Umeyama and Gerritsen 1992; Guo and Julien 2002; Absi 2011; Kundu and Ghoshal 2012; Lassabatere et al. 2012; Lu et al. 2018) or concentration distribution (Rouse 1937; Lane and Kalinske 1941; Hunt 1954; Umeyaina 1992; Huang et al. 2008; Ghoshal and Kundu 2013; Pal and Ghoshal 2017). But velocity and concentration are interrelated, and therefore need not separate but simultaneous treatment, which has been done by few (Tsai and Tsai 2000; Mazumder and Ghoshal 2002; Pal and Ghoshal 2016b), possibly due to complexity in modeling. Few researchers (Villaret and Trowbridge 1991; Ghoshal and Mazumder 2005) included sediment-induced stratification in their models, which is an important effect in a flow carrying sediments.

Density of a water-sediment mixture decreases with increasing elevation from the bed, and this stable stratification causes turbulent mixing of both momentum and sediment mass along the vertical. In brief, stratification effects lead to a velocity profile that increases faster than the logarithmic profile along a vertical and lead to a concentration profile that decreases faster than the Rousean profile along a vertical. Smith (1975) and Smith and McLean (1977a, b)

[1]Junior Research Scholar, Dept. of Mathematics, Indian Institute of Technology Kharagpur, Kharagpur 721302, India. Email: shivmohan58@gmail.com

[2]Senior Research Scholar, Dept. of Mathematics, Indian Institute of Technology Kharagpur, Kharagpur 721302, India. Email: manotosh.kumbhakar@gmail.com

[3]Associate Professor, Dept. of Mathematics, Indian Institute of Technology Kharagpur, Kharagpur 721302, India (corresponding author). Email: koeli@maths.iitkgp.ac.in

[4]Associate Professor, Dept. of Mathematics, Indian Institute of Technology Kharagpur, Kharagpur 721302, India. Email: jkumar@maths.iitkgp.ac.in

Note. This manuscript was submitted on December 18, 2018; approved on March 25, 2019; published online on September 13, 2019. Discussion period open until February 13, 2020; separate discussions must be submitted for individual papers. This paper is part of the ***Journal of Engineering Mechanics***, © ASCE, ISSN 0733-9399.

can be considered the first to make a quantitative formulation on stratification effects based on simple algebraic closures. The effect is expressed through flux Richardson number (Wright and Parker 2004; Garcia 2008), which clearly shows that the greater the amount of sediment present in the flow, the stronger the effect of stratification.

Apart from stratification effects, the sediment present in the suspension increases the density of the fluid, leading to an increment in the buoyancy force; as a result, the particle settling velocity is substantially reduced. Maude and Whitmore (1958) designated this phenomenon as hindered settling. Thacker and Lavelle (1977) incorporated the effect of concentration in the settling velocity through a factor $(1-c)^{n_H}$ multiplied by the clear-water settling velocity ω_0, where c is the concentration per unit volume and n_H is the exponent of the reduction in fall velocity. Later, many researchers (Lavelle and Thacker 1978; Woo et al. 1988; Winterwerp et al. 1990; Jing et al. 2018; Pal and Ghoshal 2013) showed the importance of including this effect in the vertical distribution of concentration. Very few researchers (Ghoshal and Mazumder 2005) used both stratification and the hindered settling effect to model velocity and concentration. But inclusion of these effects in the model of velocity and concentration led researchers to go for numerical solutions only. In fact, all other aforementioned developments are based on mainly numerical solutions.

Analytical and numerical methods are the two ways to solve a mathematical problem, and both methods have advantages and disadvantages. Due to complexity in sediment-transport models, researchers avoid going for an analytical solution. Herrmann and Madsen (2007) took into account the one-dimensional diffusion equation including the effect of stratification and went for an analytical solution of vertical concentration and closed-form solution of velocity considered together. They neglected several important factors in their modeling, maybe in order to achieve an analytical solution. The stratification effect is more pronounced in highly concentrated flow where the one-dimensional diffusion equation must be replaced by continuity equations for sediment and water separately, as presented first by Hunt (1954). Herrmann and Madsen (2007) considered the stratification effect but used the simple one-dimensional diffusion equation and also neglected the effect of hindered settling. They used several fitting parameters to match their model with laboratory experimental data. The present study mainly makes an extension to the work of Herrmann and Madsen (2007) by using the Hunt's diffusion equation as the governing equation taking into account both velocity and concentration equations simultaneously including stratification and hindered settling effect together with the nonequality of sediment and momentum diffusion coefficient and attempts to provide an approximate series solution despite the complexity of the problem.

To deal with the system of nonlinear odes developed in the present study to determine vertical velocity and concentration profiles, a novel unified method known as homotopy analysis method (HAM) developed by Liao (1992) has been adopted. The classical perturbation method (Nayfeh 2011) and asymptotic method (Grasman 2012; Lagerstrom 2013), among others, have been widely used to obtain analytical approximations of nonlinear problems that arise in science and engineering. But these methods have limitations because they are strongly dependent on small/large parameters, and their validity is confined to weakly nonlinear problems. In contrast, in the last two decades, HAM has extensively been used to deal with a variety of strong nonlinear problems such as (1) finding purely analytic and uniformly valid analytic solution of the two-dimensional (2D) laminar viscous flow over a semi-infinite flat plate (Liao 1999a, b); (2) deriving a solution for the classical problem of nonlinear progressive waves in deep water (Liao and Cheung 2003); (3) solving the generalized Benjamin-Bona-Mahony (BBM) equation (Abbasbandy 2008); (4) solving the nonlinear Riccati differential equation with fractional order (Cang et al. 2009); (5) studying convective heat transfer in a nanofluid flow over a stretching surface (Vajravelu et al. 2011); (6) analyzing elliptic differential equations and related boundary-value problems (Van Gorder 2012); (7) investigating steady-state resonance of multiple surface gravity waves in deep water (Liu and Liao 2014); (8) gaining the wave profiles of the limiting Stokes waves (Zhong and Liao 2018); and (9) solving one-dimensional time-fractional advection-dispersion equations (Singh et al. 2017), among others.

Indeed, the method is a unified one that logically contains Lyapunov's small artificial parameter method (Lyapunov 1992), Adomian decomposition method (Adomian 2013), homotopy perturbation method (HPM) (He 1999; Massa et al. 2011), δ-expansion method (Karmishin et al. 1990), and the Euler transform (Agnew 1944) as special cases. On the other hand, to the best of the authors' knowledge, HAM was applied successfully in sediment-transport problem for the first time by Kumbhakar et al. (2018), who provided an explicit analytical solution for the generalized diffusion equation. The present study aims to extend the applicability of HAM to the area of sediment transport by solving the coupled nonlinear equations for velocity and concentration with stratification and hindered settling effects. The derived approximate series solution has been validated with a numerical solution and also compared with laboratory experimental data. The importance of incorporation of stratification and hindered settling mechanism has been made clear through graphical representation and discussion.

Mathematical Modeling

Governing Equation

A sediment-laden flow of depth h in a wide open channel in which the time-averaged velocity and suspended-sediment concentration, along with the eddy viscosity, vary in the vertical direction from the reference level to the water surface is presented schematically in Fig. 1. In a steady uniform sediment-laden turbulent flow in an open channel, the equation for suspended-sediment concentration derived by Hunt (1954) considering the solid phase and fluid phase separately is

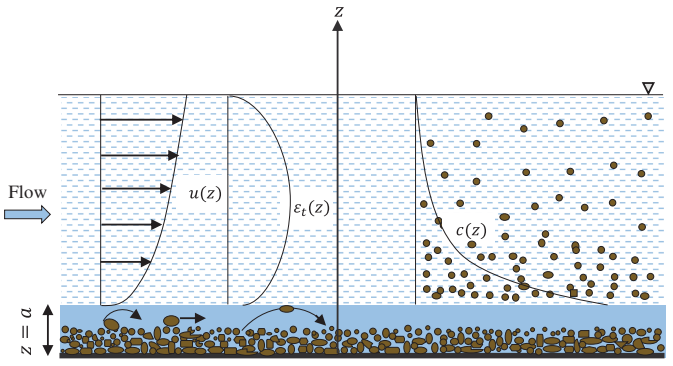

Fig. 1. Schematic diagram of velocity, eddy viscosity, and sediment concentration distribution along a vertical in an open-channel turbulent flow over a sediment bed. Within the reference level, i.e., $z \le a$, sediments move as bed load and above that as suspended load.

$$\epsilon_s \frac{dc}{dz} + (\epsilon_t - \epsilon_s)c\frac{dc}{dz} + \omega_s c(1-c) = 0 \quad (1)$$

where c = volumetric suspended sediment concentration; ϵ_s and ϵ_t = sediment diffusivity and turbulent diffusivity, respectively; and ω_s = terminal fall velocity of sediment particles. The ratio of ϵ_s to ϵ_t is called the inverse of the Schmidt number, and in the present work, it is denoted by α. Mostly, researchers consider α to be a constant over the entire flow depth and assume it to be 1 for computational conveniences. However, researchers concluded based on experimental results that α-values are different for different-sized particles (Rijn 1984; Majumdar and Carstens 1967; Jobson and Sayre 1970; Coleman 1970). Therefore, the assumption $\alpha \approx 1$ may not be physically realistic but rather a crude approximation for easy calculation. Apart from parameter α, the other parameter present in Eq. (1) is the settling velocity ω_s for a sediment particle whose magnitude is lower in the presence of surrounding particles compared with that in clear fluid. This phenomenon is commonly known as the hindered settling mechanism, and regarding this, the following expression proposed by Richarson and Zaki (1954) has been widely used:

$$\omega_s = \omega_0(1-c)^{n_H} \quad (2)$$

where ω_0 = settling velocity of sediment in clear fluid; and n_H = exponent of reduction of settling velocity. Therefore, for sediment-laden flow, the present study considers Eq. (2) in the governing Eq. (1).

The governing equation for time-averaged velocity in a steady turbulent flow can be written from Boussinesq approximation

$$\epsilon_t \frac{du}{dz} = u_*^2\left(1 - \frac{z}{h}\right) \quad (3)$$

where $u_* = \sqrt{|\tau_0|/\rho}$ is the shear velocity, where τ_0 is the bed shear stress and ρ is the fluid density; and h = maximum flow depth.

The suspended-sediment concentration decreases along a vertical; as a result, the mass density of the sediment-fluid mixture also decreases with an increase in elevation above the bed. In particular, the region near the bed having a high sediment concentration is known as the heavy fluid zone, and the rest of the region where the concentration is relatively low is known as the light fluid zone (Dey 2014). As such, the whole region behaves like a stably stratified flow region, due to which the process of turbulent mixing of the fluid momentum and the sediment mass in vertical slows down. As a result, the expressions for the distribution of both the flow velocity and the sediment concentration are modified because the sediment concentration decreases and flow velocity increases rapidly in vertical. Smith and McLean (1977b) expressed the sediment diffusivity and turbulent diffusivity by incorporating the effect of stratification in the following forms, respectively:

$$\epsilon_s = \epsilon_{s_0}(1 - \beta R_f) \quad (4)$$

$$\epsilon_t = \epsilon_{t_0}(1 - \beta R_f) = \frac{\epsilon_{s_0}}{\alpha}(1 - \beta R_f) \quad (5)$$

where ϵ_{t_0} and ϵ_{s_0} = neutral turbulent and sediment diffusivity, respectively; β = stratification correction parameter; and R_f = flux Richardson number, which can be expressed as follows (Monin and Yaglom 1971):

$$R_f = -\frac{g\Delta\epsilon_s \frac{dc}{dz}}{\epsilon_t\left(\frac{du}{dz}\right)^2} \quad (6)$$

where g = gravitational acceleration; and $\Delta = (\rho_s/\rho) - 1$, where ρ_s is sediment density and ρ is fluid density.

Substituting the expressions of ϵ_s and ϵ_t given by Eqs. (4) and (5) into Eqs. (1) and (3), one obtains the following system of two coupled odes:

$$\epsilon_{t_0}(1 - \beta R_f)[\alpha + (1-\alpha)c]\frac{dc}{dz} + \omega_0 c(1-c)^{n_H+1} = 0 \quad (7)$$

$$\epsilon_{t_0}(1 - \beta R_f)\frac{du}{dz} = u_*^2\left(1 - \frac{z}{h}\right) \quad (8)$$

Eqs. (7) and (8) represent the vertical distribution of suspended-sediment concentration and fluid velocity in a steady turbulent flow. It can be seen from Eqs. (7) and (8) that the determination of u and c needs the expression for neutral turbulent diffusivity. The available profiles of ϵ_{t_0} are of three types: constant, linear, and parabolic (Rijn 1984). Of these, the parabolic profile estimates experimental data better than the others (Graf and Cellino 2002). Therefore, the following expression is considered for neutral turbulent diffusivity:

$$\epsilon_{t_0} = \kappa u_* z\left(1 - \frac{z}{h}\right) \quad (9)$$

By substituting dc/dz, du/dz, ϵ_s, ϵ_t, and ϵ_{t_0} given by Eqs. (1), (3)–(5), and (9), respectively, into Eq. (6), after some algebraic calculations, the following are obtained:

$$R_f = \frac{\gamma\alpha z c(1-c)^{n_H+1}}{(1-\frac{z}{h})[\alpha + (1-\alpha)c] + \beta\gamma\alpha z c(1-c)^{n_H+1}} \quad (10)$$

$$\Rightarrow 1 - \beta R_f = \frac{(1-\frac{z}{h})[\alpha + (1-\alpha)c]}{(1-\frac{z}{h})[\alpha + (1-\alpha)c] + \beta\alpha\gamma z c(1-c)^{n_H+1}} \quad (11)$$

where $\gamma = \kappa g\Delta\omega_0/u_*^3$. Replacing $1 - \beta R_f$ in Eqs. (7) and (8) and making the equations nondimensional by using the reference concentration c_a, shear velocity u_*, and maximum flow depth h, the governing equations in the simplified form are obtained as follows:

$$\begin{aligned}&\kappa u_*\xi(1-\xi)^2[\alpha + (1-\alpha)c_a C]^2\frac{dC}{d\xi} \\ &\quad + \omega_0 C(1-c_a C)^{n_H+1}((1-\xi)[\alpha + (1-\alpha)c_a C] \\ &\quad + \beta\alpha\gamma c_a h C\xi(1-c_a C)^{n_H+1}) = 0\end{aligned} \quad (12)$$

$$\begin{aligned}&\kappa\xi(1-\xi)[\alpha + (1-\alpha)c_a C]\frac{dU}{d\xi} \\ &\quad = (1-\xi)[\alpha + (1-\alpha)c_a C] + \beta\alpha\gamma c_a h C\xi(1-c_a C)^{n_H+1}\end{aligned} \quad (13)$$

where the nondimensionalization is done as follows: $\xi = z/h$, $C = c/c_a$, and $U = u/u_*$.

Boundary Conditions

To solve coupled equations Eqs. (12) and (13) simultaneously, specified values of u and c are required at a common elevation, say $z = a$, which is termed the reference level in the present study. To that end, the following boundary conditions are prescribed:

$$c(z = a) = c_a \quad (14)$$

$$u(z = a) = u_a \quad (15)$$

where c_a and u_a = reference concentration and reference velocity, respectively. Boundary conditions are made dimensionless as follows:

$$C(\xi = \xi_a) = 1 \tag{16}$$

$$U(\xi = \xi_a) = \frac{u_a}{u_*} \tag{17}$$

where ξ_a = dimensionless reference level defined as $\xi_a = a/h$.

It can be seen that the coupled odes given by Eqs. (12) and (13) are highly nonlinear due to the power term $(1 - c_a C)^{n_H+1}$. The primary objective of this study is to find an analytical solution to that system, which essentially needs special mathematical treatment such as that presented in the next section.

Approximate Series Solution Based on HAM

Liao (1992) proposed an approximate analytical method known as the homotopy analysis method, which is essentially based on the idea of homotopy, a fundamental concept in topology, for solving strongly nonlinear problems. The methodology of HAM is explained for solving the system of nonlinear ordinary differential equations. For that purpose, let the system be written as follows:

$$\mathcal{N}_i[y_i(\xi)] = 0, \quad i = 1, 2, \ldots, n \tag{18}$$

where $\mathcal{N}_i$ = nonlinear operators; ξ = independent variable; $y_i(\xi)$ = unknown functions that need to be determined; and n = number of equations in the system. Liao (1992) constructed the so-called zero-order deformation equation by generalizing the traditional homotopy as follows:

$$(1 - q)\mathcal{L}_i[\Phi_i(\xi; q) - y_{i,0}(\xi)] - q h_i H_i(\xi)\mathcal{N}_i[\Phi_i(\xi; q)] = 0 \tag{19}$$

with the boundary conditions

$$\Phi_i(\xi_a; q) = y_i(\xi = \xi_a) \tag{20}$$

where $\mathcal{L}_i$ = auxiliary linear operators with the property that

$$\mathcal{L}_i g = 0 \quad \text{when } g = 0 \tag{21}$$

where $\Phi_i(\xi; q)$ = unknown functions; $y_{i,0}(\xi)$ = initial approximations of $y_i(\xi)$; h_i = nonzero auxiliary parameters known as convergence control parameters that control the rate of convergence of the series; $H_i(\xi)$ not equal to zero ($\neq$) 0 = auxiliary functions; and $q \in [0, 1]$ = embedding parameter such that as q increases from 0 to 1, $\Phi_i(\xi; q)$ varies from initial approximations $y_{i,0}(\xi)$ to the exact solutions $y_i(\xi)$ of the nonlinear equations. Mathematically, it can be written as follows:

$$\Phi_i(\xi; 0) = y_{i,0}(\xi) \quad \text{and} \quad \Phi_i(\xi; 1) = y_i(\xi) \tag{22}$$

Due to the dependency of $\Phi_i(\xi; q)$ on q, it can be expand in Taylor series about $q = 0$ as follows:

$$\Phi_i(\xi; q) = \Phi_i(\xi; 0) + \sum_{m=1}^{\infty} y_{i,m}(\xi) q^m \tag{23}$$

where

$$y_{i,m}(\xi) = \frac{1}{m!}\frac{\partial^m \Phi_i(\xi; q)}{\partial q^m}\bigg|_{q=0} \tag{24}$$

known as mth-order deformation derivatives. According to Liao (2003), the convergence behavior of the series totally depends on the selection of linear operators $\mathcal{L}_i$, auxiliary parameters h_i, auxiliary functions $H_i(\xi)$, and initial approximations $y_{i,0}(\xi)$. Assuming that $\mathcal{L}_i$, h_i, $H_i(\xi)$, and $y_{i,0}(\xi)$ are chosen in such a way that the series Eq. (23) converges at $q = 1$, then at $q = 1$, Eq. (23) becomes

$$\Phi_i(\xi; 1) = \Phi_i(\xi; 0) + \sum_{m=1}^{\infty} y_{i,m}(\xi) \tag{25}$$

Using Eq. (22), series Eq. (25) becomes

$$y_i(\xi) = y_{i,0}(\xi) + \sum_{m=1}^{\infty} y_{i,m}(\xi) \tag{26}$$

Eq. (26) provides a relationship between the initial guesses $y_{i,0}(\xi)$ and final solutions $y_i(\xi)$ through the higher-order terms $y_{i,m}(\xi)$. The higher-order terms $y_{i,m}(\xi)$ for $m \geq 1$ can be obtained by differentiating the zero-order deformation equation Eq. (19) m times with respect to embedding parameter q, setting $q = 0$, and then dividing by $m!$ as follows:

$$\mathcal{L}_i[y_{i,m}(\xi) - \chi_m y_{i,m-1}(\xi)] = h_i H_i(\xi) R_{i,m}(\vec{y}_{i,m-1}) \tag{27}$$

subject to

$$y_{i,m}(\xi_a) = 0 \tag{28}$$

where

$$\chi_m = \begin{cases} 0 & \text{if } m \leq 1 \\ 1 & \text{otherwise} \end{cases} \tag{29}$$

and

$$R_{i,m}(\vec{y}_{i,m-1}) = \frac{1}{(m-1)!}\frac{\partial^{m-1}\mathcal{N}_i[\Phi_i(\xi; q)]}{\partial q^{m-1}}\bigg|_{q=0} \tag{30}$$

It can be seen from Eq. (26) that HAM transfers the original nonlinear problem governed by Eq. (18) into infinitely many linear subproblems through its higher-order deformation Eq. (27) together with the boundary conditions Eq. (28). The solution can then be approximated up to a finite number of terms, i.e., as follows:

$$y_i(\xi) \approx \sum_{n=0}^{m} y_{i,n}(\xi) \tag{31}$$

which is known as the mth-order approximation of HAM. The methodology has great freedom to choose $\mathcal{L}_i$, $H_i(\xi)$, and $y_{i,0}(\xi)$, as shown by Liao (2003), who also proposed some fundamental rules such as the rule of solution expression, rule of coefficient ergodicity, and rule of solution existence, to assist in the selection.

In the present study, two coupled nonlinear odes governed by Eqs. (12) and (13) subject to the boundary condition Eqs. (16) and (17) are to be solved by HAM. For that purpose, let the solutions $C(\xi)$ and $U(\xi)$ be represented by the following set of base functions:

$$\{\xi^n[\ln(\xi)]^m : n, m = 0, 1, 2, \ldots,\} \tag{32}$$

in the form of

$$C(\xi) = \sum_{n=0}^{\infty}\sum_{m=0}^{\infty} c_{n,m}\xi^n[\ln \xi]^m \tag{33}$$

and

J. Eng. Mech., 2019, 145(11): 04019090

$$U(\xi) = \sum_{n=0}^{\infty}\sum_{m=0}^{\infty} d_{n,m}\xi^n[\ln \xi]^m \tag{34}$$

where $c_{n,m}$ and $d_{n,m}$ = coefficients. According to the rule of solution expression and the given boundary condition Eqs. (16) and (17), one can simply choose

$$y_{1,0}(\xi) = 1 \quad \text{and} \quad y_{2,0}(\xi) = \frac{u_a}{u_*} + \lambda(\xi - \xi_a) \tag{35}$$

as the initial approximations of $C(\xi)$ and $U(\xi)$, respectively, where λ = additional convergence control parameter that needs to be determined. The auxiliary linear operators are chosen as follows:

$$\mathcal{L}_1[\Phi_1(\xi;q)] = \xi\frac{\partial\Phi_1(\xi;q)}{\partial\xi} \tag{36}$$

and

$$\mathcal{L}_2[\Phi_2(\xi;q)] = \xi\frac{\partial\Phi_2(\xi;q)}{\partial\xi} \tag{37}$$

with the property that

$$\mathcal{L}_i[A_i] = 0, \quad i = 1,2 \tag{38}$$

where A_i = constants.

Nonlinear operators are expressed as follows:

$$\begin{aligned}\mathcal{N}_1[\Phi_1(\xi;q),\Phi_2(\xi;q)] &= \kappa u_*\xi(1-\xi)^2[\alpha+(1-\alpha)c_a\Phi_1]^2\frac{d\Phi_1}{d\xi} + \omega_0\Phi_1(1-c_a\Phi_1)^{n_H+1} \\ &\times((1-\xi)[\alpha+(1-\alpha)c_a\Phi_1] + \beta\alpha\gamma c_a h\xi\Phi_1(1-c_a\Phi_1)^{n_H+1})\end{aligned} \tag{39}$$

$$\begin{aligned}\mathcal{N}_2[\Phi_1(\xi;q),\Phi_2(\xi;q)] &= \kappa\xi(1-\xi)[\alpha+(1-\alpha)c_a\Phi_1]\frac{d\Phi_2}{d\xi} \\ &- (1-\xi)[\alpha+(1-\alpha)c_a\Phi_1] \\ &+ \beta\alpha\gamma c_a h\xi\Phi_1(1-c_a\Phi_1)^{n_H+1}\end{aligned} \tag{40}$$

For simplicity in computation, the auxiliary functions $H_i(\xi) = 1$ are chosen for $i = 1,2$. Now applying the inverse of linear operators given by Eqs. (36) and (37) and using the boundary conditions, the higher-order terms $y_{1,m}(\xi)$ and $y_{2,m}(\xi)$ for $m \geq 1$ can be calculated according to Eq. (27) as follows:

$$y_{1,m} = \chi_m y_{1,m-1}(\xi) + h_1\int_{\xi_a}^{\xi}\frac{1}{\xi}R_{1,m}(\vec{y}_{1,m-1})d\xi \tag{41}$$

and

$$y_{2,m} = \chi_m y_{2,m-1}(\xi) + h_2\int_{\xi_a}^{\xi}\frac{1}{\xi}R_{2,m}(\vec{y}_{2,m-1})d\xi \tag{42}$$

where

$$\begin{aligned}R_{1,m}(\vec{y}_{i,m-1}) &= \kappa u_*\xi(1-\xi)^2[\alpha^2 y'_{1,m-1} \\ &+ (1-\alpha)^2 c_a^2\sum_{i=0}^{m-1}y'_{1,m-1-i}\sum_{j=0}^{i}y_{1,j}y_{1,i-j} \\ &+ 2\alpha(1-\alpha)c_a\sum_{i=0}^{m-1}y_{1,m-i-1}y'_{1,i}] \\ &+ \omega_0(1-\xi)[\hat{\mathcal{D}}_{m-1}[f_1(\Phi_1)]|_{q=0} + \hat{\mathcal{D}}_{m-1}[f_2(\Phi_1)]|_{q=0}] \\ &+ \beta\alpha\gamma c_a h\xi\hat{\mathcal{D}}_{m-1}[f_3(\Phi_1)]|_{q=0}\end{aligned} \tag{43}$$

and

$$\begin{aligned}R_{2,m}(\vec{y}_{i,m-1}) &= \kappa\xi(1-\xi)\left[\alpha y'_{2,m-1} + (1-\alpha)c_a\sum_{i=0}^{m-1}y_{1,m-i-1}y'_{2,i}\right] \\ &- (1-\xi)\alpha(1-\chi_m) - (1-\xi)(1-\alpha)c_a y_{1,m-1} \\ &- \beta\alpha\gamma h c_a\xi\hat{\mathcal{D}}_{m-1}[f_4(\Phi_1)]|_{q=0}\end{aligned} \tag{44}$$

where $\hat{\mathcal{D}}_m \equiv \frac{1}{m!}\frac{\partial^m}{\partial q^m}$, $f_1(\Phi_1) = \alpha\Phi_1(1-c_a\Phi_1)^{n_H+1}$, $f_2(\Phi_1) = (1-\alpha)c_a(\Phi_1)^2(1-c_a\Phi_1)^{n_H+1}$, $f_3(\Phi_1) = \omega_0(\Phi_1)^2(1-c_a\Phi_1)^{2(n_H+1)}$, $f_4(\Phi_1) = \Phi_1(1-c_a\Phi_1)^{n_H+1}$ and

$$\hat{\mathcal{D}}_m[f(\Phi)] = \begin{cases}\sum_{k=0}^{m-1}\left(1-\frac{k}{m}\right)\hat{\mathcal{D}}_{m-k}(\Phi)\frac{\partial}{\partial\Phi}\hat{\mathcal{D}}_k[f(\Phi)], & \text{if } m \geq 1 \\ f(\Phi), & \text{if } m = 0\end{cases} \tag{45}$$

The proof for the derivation of Eq. (45) can be found in Appendix I. Finally, the mth-order HAM-based approximation for the concentration and velocity distribution according to Eq. (31) can be written explicitly as follows, respectively:

$$C(\xi) = y_1(\xi) \approx \sum_{n=0}^{m} y_{1,n}(\xi) \tag{46}$$

and

$$U(\xi) = y_2(\xi) \approx \sum_{n=0}^{m} y_{2,n}(\xi) \tag{47}$$

For the sake of completeness, the theoretical convergence analysis for the series solutions obtained is given in Appendix II.

Results and Discussion

This section discusses the validation of approximate analytical series solutions of Eqs. (12) and (13) obtained by HAM with the numerical solution as well as with experimental data available in the literature. The rest focuses on the physical interpretation of the several turbulent mechanisms included in the model.

Validation of the HAM-Based Solution

It can be observed that the series solution expressions for suspended-sediment concentration and flow velocity obtained by HAM given by Eqs. (46) and (47), respectively, are functions of ξ, h_1, h_2, and λ. As suggested by Liao (2003), the convergence control parameters h_1, h_2, and λ play a significant role in controlling the convergence behavior of the series solutions Eqs. (46) and (47). Therefore, an appropriate choice of these convergence control parameters will lead toward the convergence of series solutions to the exact solutions. Liao (2003) proposed a h-level curve method to determine the optimal values of these parameters. However this

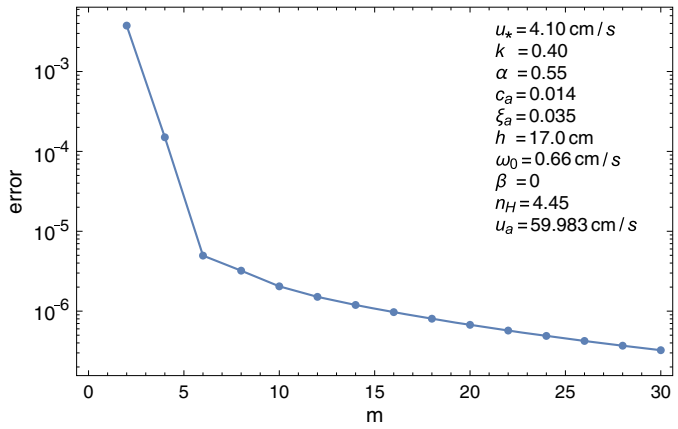

Fig. 2. Residual error [Eq. (49)] ε_m versus the order of approximation m.

method is not particularly appropriate for choosing the best optimal values of the parameters so that the series converges faster. Later, Liao (2012) proposed a new method, called the square residual error method, to determine the convergence control parameters, in which the square residual error is minimized to get the optimum value of convergence parameters. The square residual error is defined as follows:

$$\varepsilon = \int_{\xi_a}^{1} \{(\mathcal{N}_1[C(\xi), U(\xi)])^2 + (\mathcal{N}_2[C(\xi), U(\xi)])^2\} d\xi \qquad (48)$$

where $C(\xi)$ and $U(\xi) = m$th-order HAM-based solution given by Eqs. (46) and (47), respectively. To avoid the computational difficulty in integration, the square residual error can be written in discrete form as follows:

$$\varepsilon_m = \frac{1}{L+1}\left(\sum_{j=0}^{L} \{(\mathcal{N}_1[C(\xi_j), U(\xi_j)])^2 + (\mathcal{N}_2[C(\xi_j), U(\xi_j)])^2\}\right) \qquad (49)$$

where $L + 1$ = equally distributed discrete points. It was proven in a general way that as the square residual error tends to zero, the homotopy series converges to the solution of the original problem. Therefore, it is sufficient to check the residual error Eq. (49) only. A test case performed to show the behavior of the square residual error ε_m with the order of approximation of HAM-based solution is plotted in Fig. 2, where the optimum values of convergence control parameters are found as $h_1 = -0.692264$, $h_2 = -3.53594$, and $\lambda = 2.86625$. It can be observed from the figure that as the order of approximation m increases, total error of the system decreases systematically, which reveals the suitability of the chosen operators and approximations and hence the convergence behavior of the method.

Now, the HAM-based approximate analytical solutions are verified with the numerical solution. To obtain the numerical solution of the system, NDSolve of Mathematica version 11.0 is used, and a suitable set of the required parameters needed to assess the models is chosen. The function NDSolve contains many numerical methods, with the most suitable one automatically chosen by the software. Fig. 3 compares the numerical solution at some discrete points with the 30th-order HAM-based approximation. The convergence control parameters are determined from the method described in the preceding section. It can be observed from the figure that the analytic approximate solutions are closer to the numerical ones. Apart from the graphical solutions, the quantitative assessment is given in Table 1 for some discrete points of the domain, which ensures the stability of the proposed method.

Physical Interpretation of the Model

Neutral and Stratified Eddy Viscosity Profile

Eddy viscosity profile given by Eq. (5) is plotted in Fig. 4 for both the neutral and stratified cases. The magnitude of the correction factor $(1 - \beta R_f)$ is less than unity, which damps the eddy viscosity for sediment-laden flow in comparison with that of clear-water flow. Near the channel bed and water surface, the flux Richardson

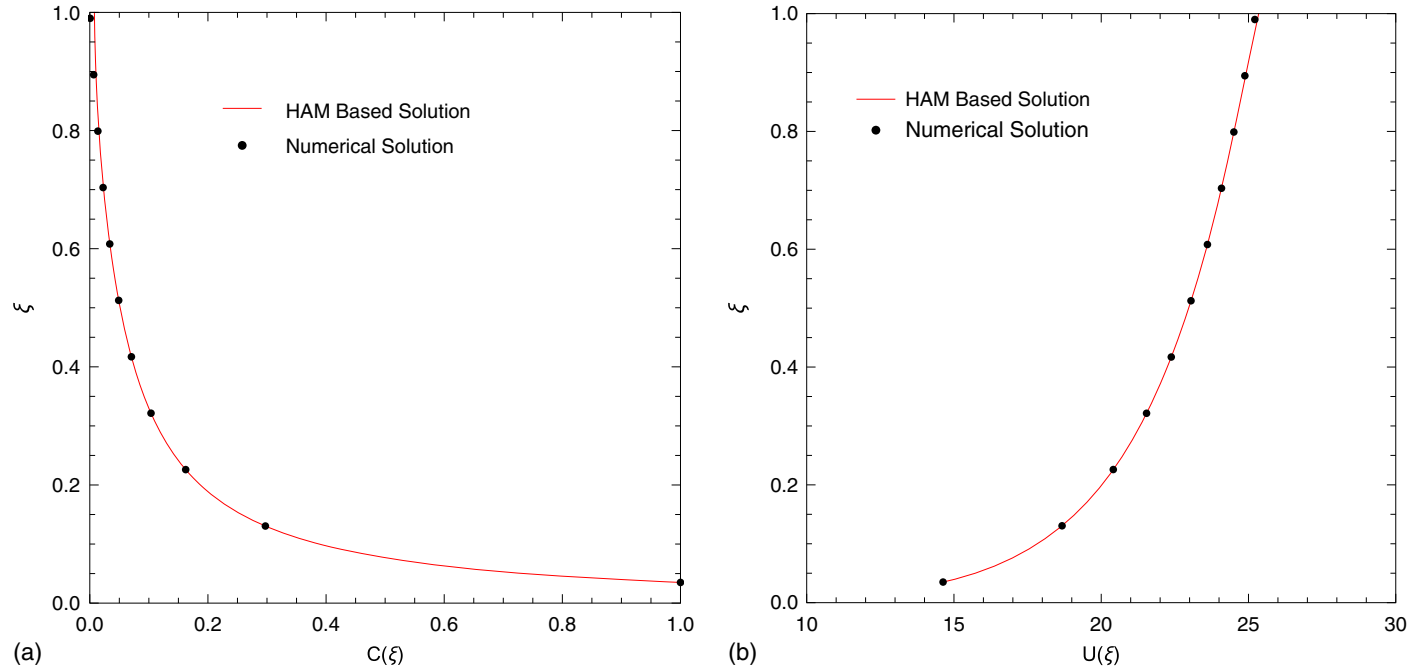

Fig. 3. Comparison of the 30th-order HAM-based approximation with numerical solution: (a) concentration profile; and (b) velocity profile.

J. Eng. Mech., 2019, 145(11): 04019090

Table 1. Comparison of the numerical solution with the different orders of approximation of HAM for $C(\xi)$ and $U(\xi)$

	Numerical solution		30th-order approximately		15th-order approximately		5th-order approximately	
ξ	$C(\xi)$	$U(\xi)$	$C(\xi)$	$U(\xi)$	$C(\xi)$	$U(\xi)$	$C(\xi)$	$U(\xi)$
0.0350	1	14.6300	1	14.6300	1	14.6300	1	14.6300
0.1305	0.297256	18.6708	0.297252	18.6708	0.296968	18.6703	0.296939	18.5995
0.2260	0.162356	20.4095	0.162354	20.4094	0.161691	20.4055	0.140884	20.3356
0.3215	0.103640	21.5387	0.103638	21.5387	0.102843	21.5295	0.082491	21.4403
0.4170	0.070437	22.3784	0.070432	22.3783	0.069536	22.3616	0.054012	22.2402
0.5125	0.048938	23.0481	0.048951	23.0477	0.048096	23.0211	0.035671	22.8647
0.6080	0.033798	23.6057	0.033945	23.6051	0.033366	23.5659	0.021806	23.3783
0.7035	0.022498	24.0840	0.023115	24.0839	0.023048	24.0298	0.012198	23.8169
0.7990	0.013689	24.5033	0.015448	24.5079	0.001599	24.4302	0.008674	24.2014
0.8945	0.006573	24.8771	0.010499	24.9008	0.011528	24.8022	0.013216	24.5440
0.9900	0.000593	25.2157	0.007946	25.2016	0.009137	25.1550	0.026559	24.8516

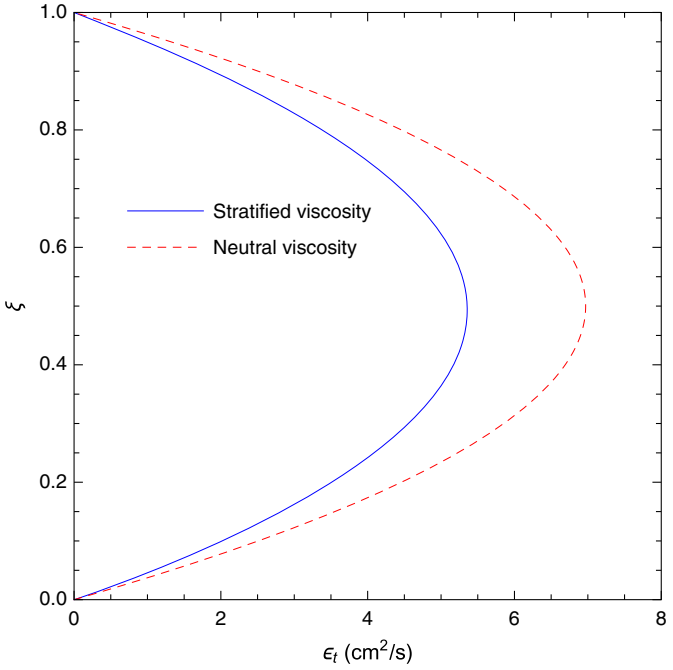

Fig. 4. Neutral and stratified eddy viscosity profile along a vertical.

number R_f takes on very small values, leading to negligible change in the relevant stratified profile.

Effect of Stratification on Fluid Velocity and Sediment Concentration

Comparison of sediment concentration and fluid velocity profiles for stratified and neutral flow is depicted in Fig. 5. The continuous line stands for $\beta = 0$, i.e., without stratification, and the dotted line stands for $\beta = 4$, i.e., with stratification. The other required parameters are given in the figures. It is known that the stratification effect dampens the sediment diffusivity; as a consequence, the sediment concentration decreases. In case of concentration, stratification effects are prominent in some specific region of the water column. Because the concentration is very small in the higher region of the water column, the density difference is not significant and the stratification effect is almost negligible there. Again, in the near-bed region, the eddies responsible for transporting momentum are very small, and therefore the stratification effect is not prominent there either. It is evident from the figure that the effect of stratification is prominent in the intermediate region of the flow. On the other hand, the decrease of turbulent diffusivity due to stratification results in increasing velocity, as can be seen from the figure.

Effect of Hindered Settling Mechanism

The effect of the hindered settling mechanism through the exponent n_H on suspended-sediment concentration and fluid velocity profiles is shown in Fig. 6, where the case $n_H = 0$, i.e., without hindered settling effect, and case $n_H \neq 0$, i.e., with hindered settling effect, are considered. It is well known that the hindered settling effect is pronounced in highly concentrated flows. To that end, a relevant set of parameters was chosen and is presented in the figure. It can be observed from Fig. 6(a) that the concentration difference is visible in the main flow region because near the water surface, the particle concentration is too low and in the near-bed region, particles are not in suspension. On the other hand, the velocity profile is affected by n_H in the upper region of the flow, as can be seen in Fig. 6(b).

Variation of Velocity and Concentration Profiles with Inverse Schmidt Number

The velocity and concentration profiles for stratified flow with different inverse Schimdt numbers are plotted in Fig. 7. Five different values of α are chosen to assess the profiles. It can be observed from the figure that both the velocity and concentration values increase with the increase of α. The increasing pattern for concentration profile becomes convex to concave type, and shifted increasing behavior is observed for velocity. For a certain region of the flow zone, specifically for $\xi \leq 0.2$, both profiles are convergent in nature. Further, it has been observed that the profiles' changing behavior is less sensitive to α in comparison with that of neutral flow.

Comparison with Experimental Data

Finally, the derived profiles are validated with the available experimental data in the literature. The theoretical formulation of the present work is a generalization of the work of Herrmann and Madsen (2007). Unlike them, the approach proposed here started with the Hunt's diffusion equation, and the settling velocity of a sediment particle is considered to be a function of sediment concentration instead of assuming it to be a constant. Therefore, the derived models are also valid for highly concentrated flows. For that purpose, two kinds of experimental data are considered: dilute flow from Coleman (1981) and nondilute flow from Einstein and Chien (1955).

Coleman (1981) used a 356-mm-wide and 15-m-long smooth flume. The flow depth was maintained near about 17.1 cm. Test cases 1, 21, and 32 out of 40 test cases were performed in clear-water flow and Test cases 2–20 were performed over a

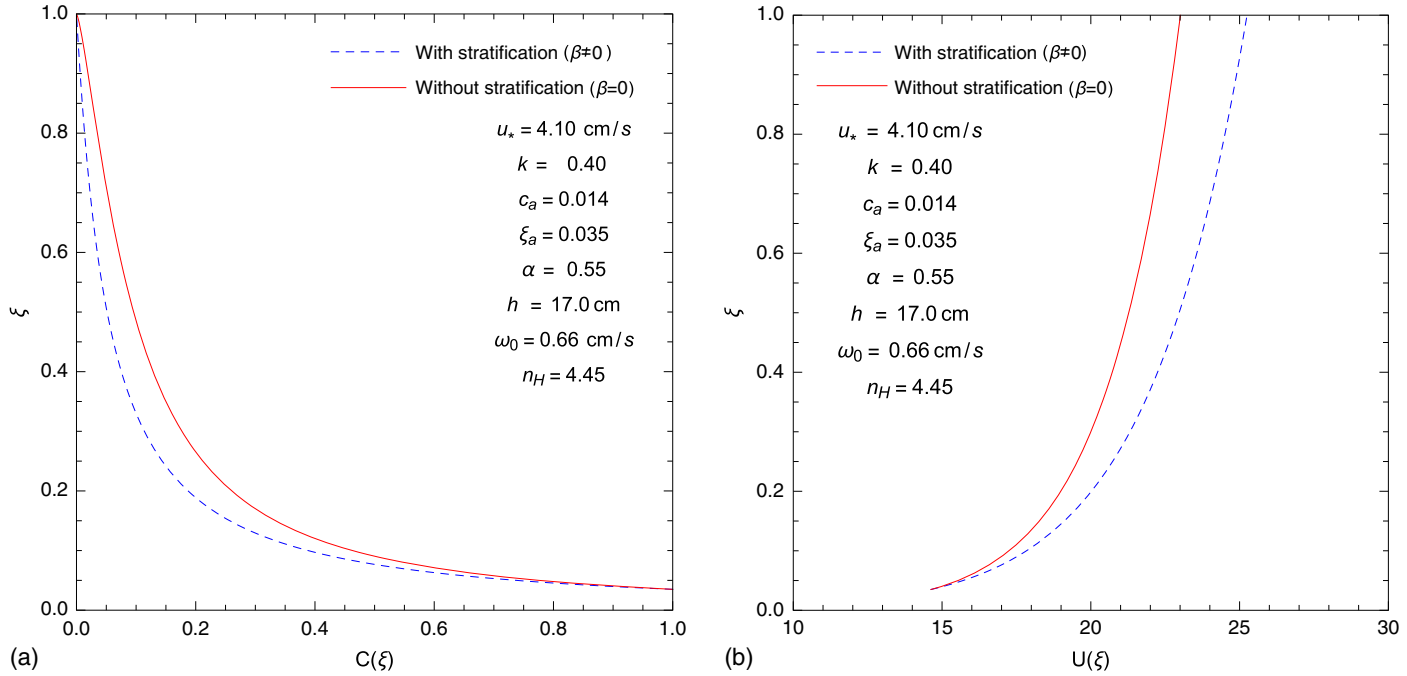

Fig. 5. Profiles for stratified and the neutral flow: (a) concentration profile; and (b) velocity profile. Dashed line represents stratified with $[\alpha, \beta] = [0.55, 4]$, and solid line represents neutral with $[\alpha, \beta] = [0.55, 0]$.

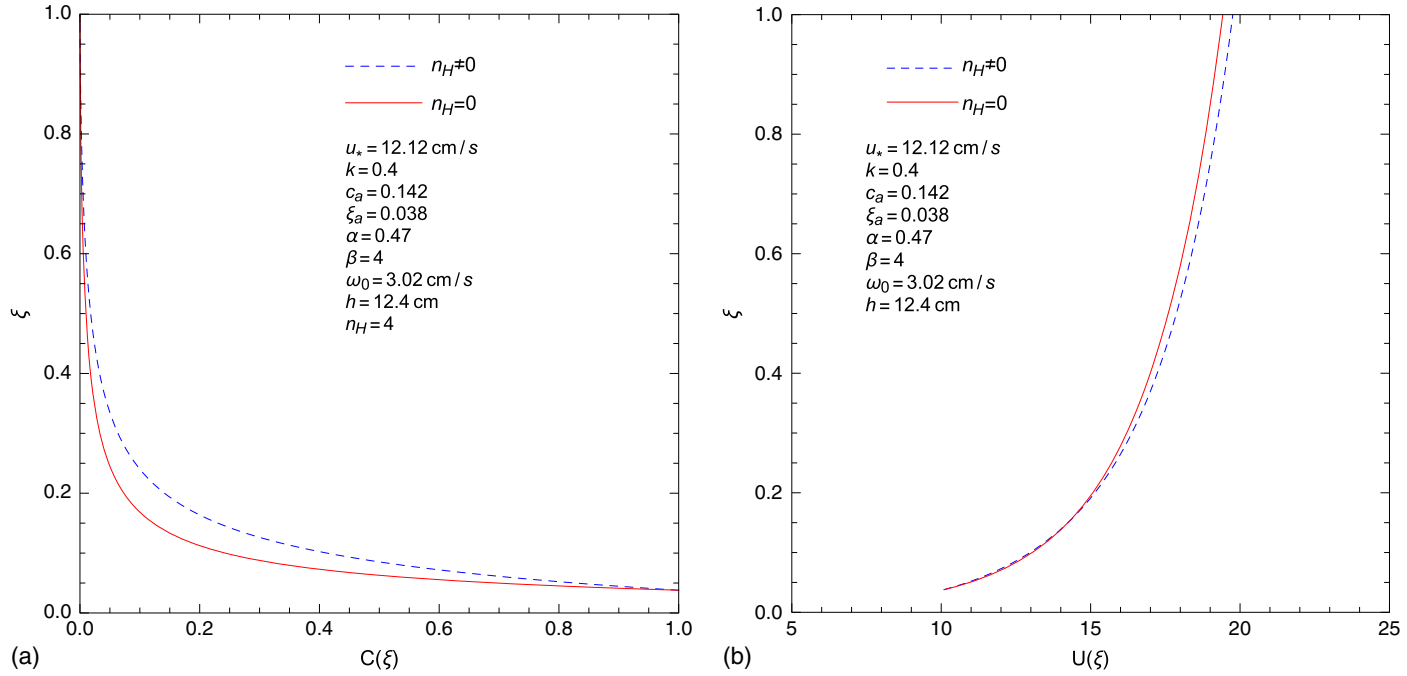

Fig. 6. Effect of n_H on the models: (a) concentration profile; and (b) velocity profile.

sediment bed with three different sand diameters $d = 0.105$, $d = 0.21$, and $d = 0.42$ mm. In contrast, Einstein and Chien (1955) performed experiments very close to the channel bed and reported 16 different measurement runs, named Run S1 to S16 for three different particle diameters of 1.3, 0.940, and 0.274 mm.

It can be observed that to determine the velocity and concentration profiles, several parameters, such as clear-water settling velocity ω_0, inverse Schmidt number α, and exponent of reduction of fall velocity n_H, need to be calculated. For that purpose, ω_0 is computed from the well-known expression given by Cheng (1997) as follows:

$$\omega_0 = \frac{\nu_f}{d}\left(\sqrt{25 + 1.2d_*^2} - 5\right)^{1.5} \tag{50}$$

where ν_f = kinematic viscosity of clear fluid; and d_* = dimensionless particle diameter defined by $d_* = (\Delta g/\nu_f^2)^{1/3} d$,

J. Eng. Mech., 2019, 145(11): 04019090

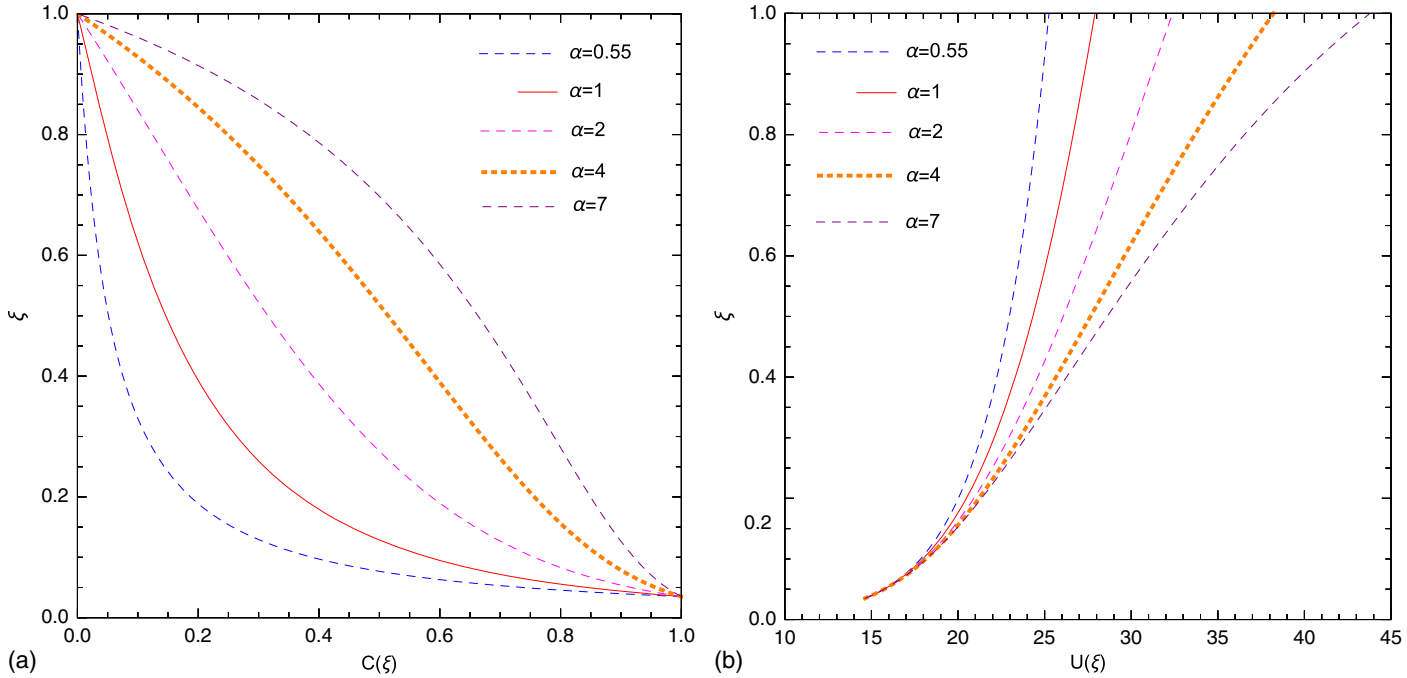

Fig. 7. Variation of the models for different values of α: (a) concentration profile; and (b) velocity profile.

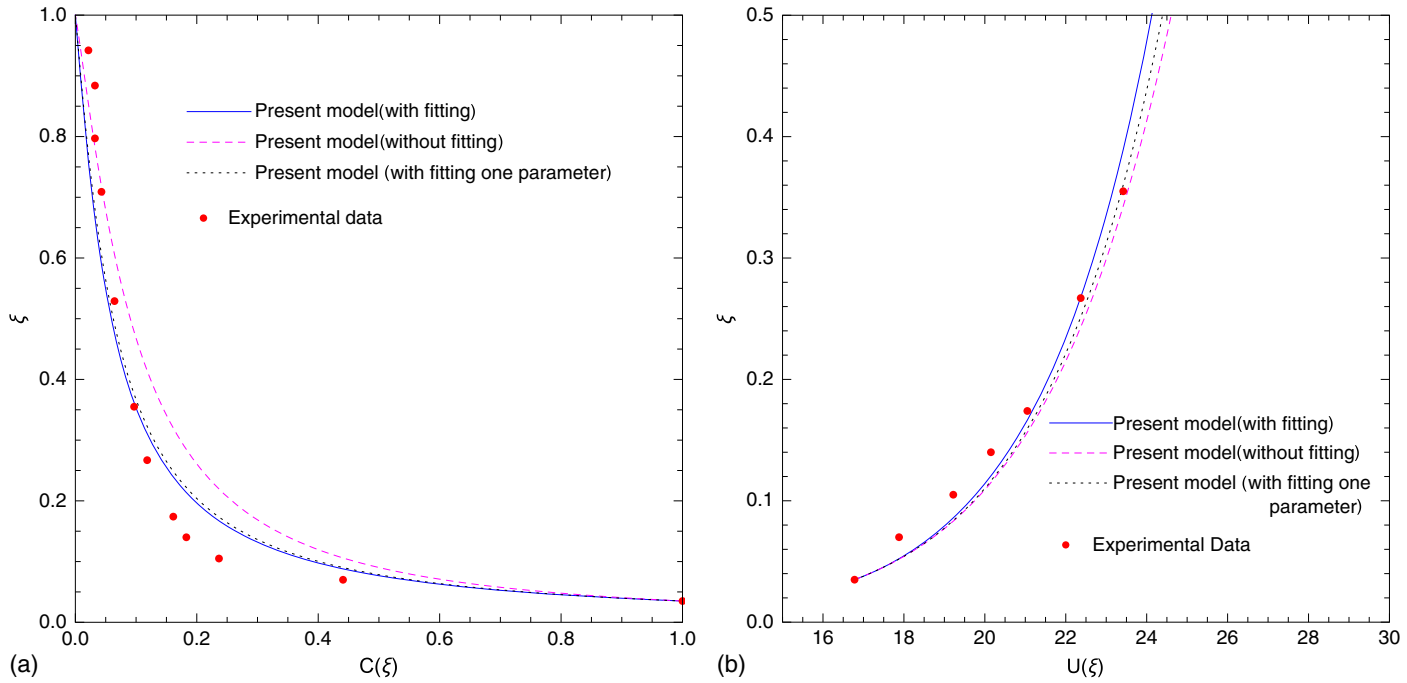

Fig. 8. Comparison of derived models with Run 35 of Coleman (1981) : (a) concentration profile; and (b) velocity profile. Continuous line stands for the present model with both α and β as fitting parameters, dotted line represents the models with one parameter fixed and the other varying ($\alpha = 4.23$ and $\beta = 4$), dashed line stands for the present model without fitting procedure, and the dots stand for the experimental data.

where d is the particle diameter. On the other hand, the literature on the expression of α is limited (Rijn 1984; Pal and Ghoshal 2016a). The expression was selected from a recent study by Pal and Ghoshal (2016a), who showed that α values depend on the reference level and reference concentration along with the normalized settling velocity. By analyzing a wide range of experimental data, they developed the following expressions:

$$\alpha = \begin{cases} 0.033\left(\frac{\omega_0}{u_*}\right)^{0.931}\xi_a^{-1.196}c_a^{-0.118} & \text{for dilute flows} \\ 2.204\left(\frac{\omega_0}{u_*}\right)^{0.667}\xi_a^{0.178}c_a^{0.017} & \text{for nondilute flows} \end{cases} \quad (51)$$

The exponent n_H depends mainly on the particle Reynolds number (Richarson and Zaki 1954; Chien and Wan 1999; Garside and Al-Dibouni 1977). There are many formulas available for the

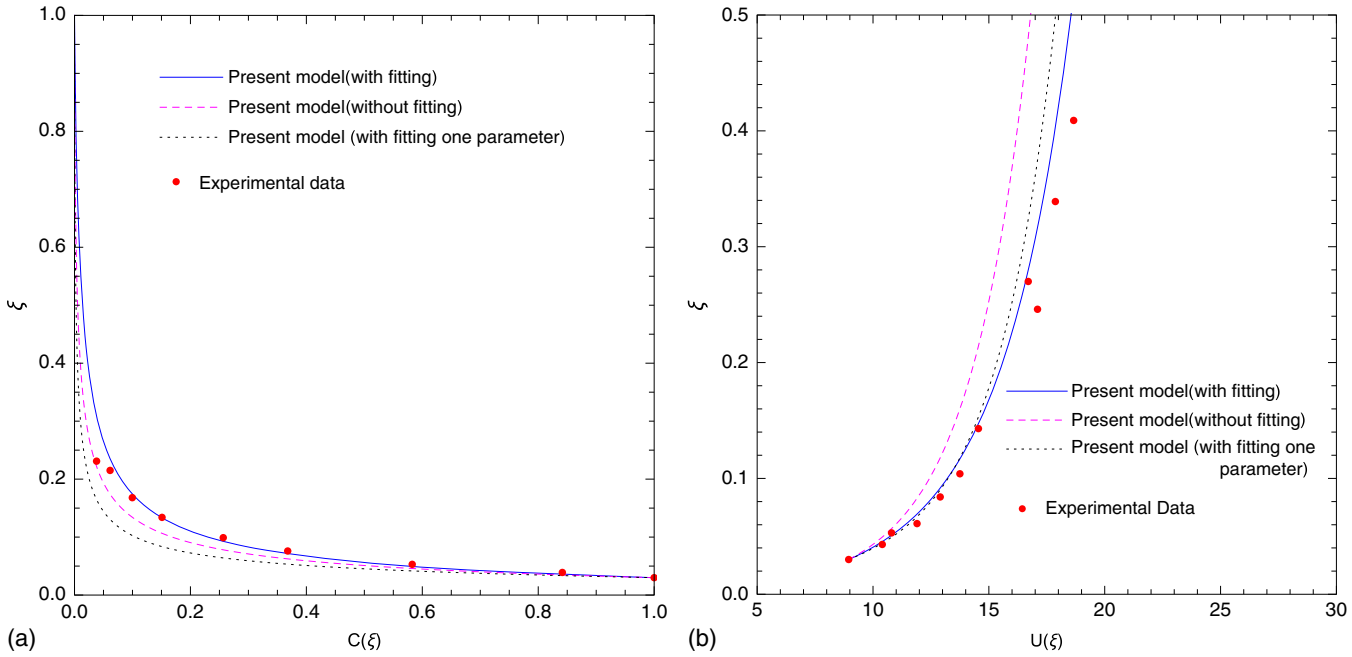

Fig. 9. Comparison of derived models with Run S12 of Einstein and Chien (1955): (a) concentration profile; and (b) velocity profile. Continuous line stands for the present model with both α and β as fitting parameters, dotted line represents the models with one parameter fixed and the other varying ($\alpha = 0.5056$ and $\beta = 13.01$), dashed line stands for the present model without fitting procedure, and the dots stand for the experimental data.

expression of n_H. The present study uses the formula given by Richarson and Zaki (1954) as follows:

$$n_H = \begin{cases} 4.65 & \text{when } Re_p < 0.2 \\ 4.4Re_p^{-0.03} & \text{when } 0.2 < Re_p < 1 \\ 4.4Re_p^{-0.1} & \text{when } 1 < Re_p < 500 \\ 2.4 & \text{when } 500 < Re_p \end{cases} \tag{52}$$

in which $Re_p = \omega_0 d/\nu_f$.

Two different runs, namely Run 35 of Coleman (1981) and Run S12 of Einstein and Chien (1955), were chosen for comparison of the present models. In Figs. 8 and 9, the derived models are considered for three cases: (1) fixed $\beta = 4$ and α given by Eq. (51), (2) one parameter fixed and the other varying, and (3) fitting both α and β with the data. Because in the experimental data of Coleman (1981), the dip phenomenon was observed, which comes due to the wake and secondary current effects, and the proposed model does not incorporate these effects, velocity data up to 50% of the flow depth, i.e., $\xi \leq 0.5$, were considered.

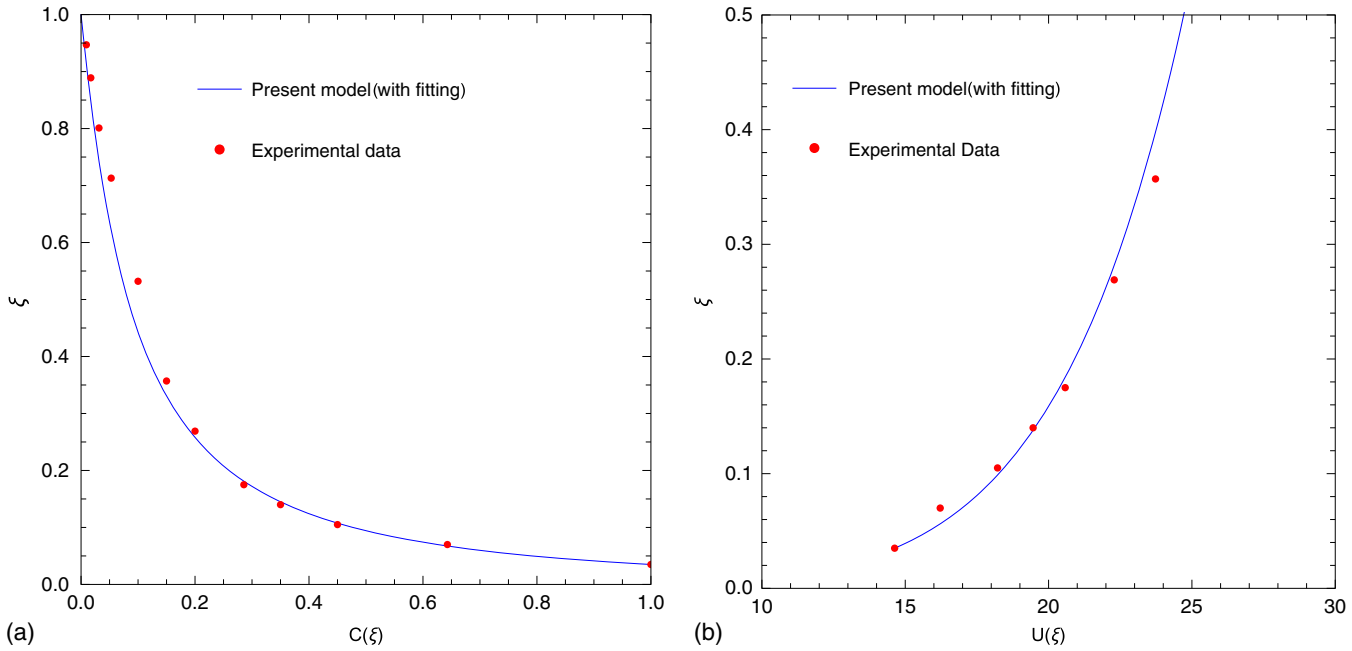

Fig. 10. Comparison of derived models with Run 13 of Coleman (1981): (a) concentration profile; and (b) velocity profile. Continuous line stands for the present model with α and β as fitting parameters, and the dots stand for the experimental data.

J. Eng. Mech., 2019, 145(11): 04019090

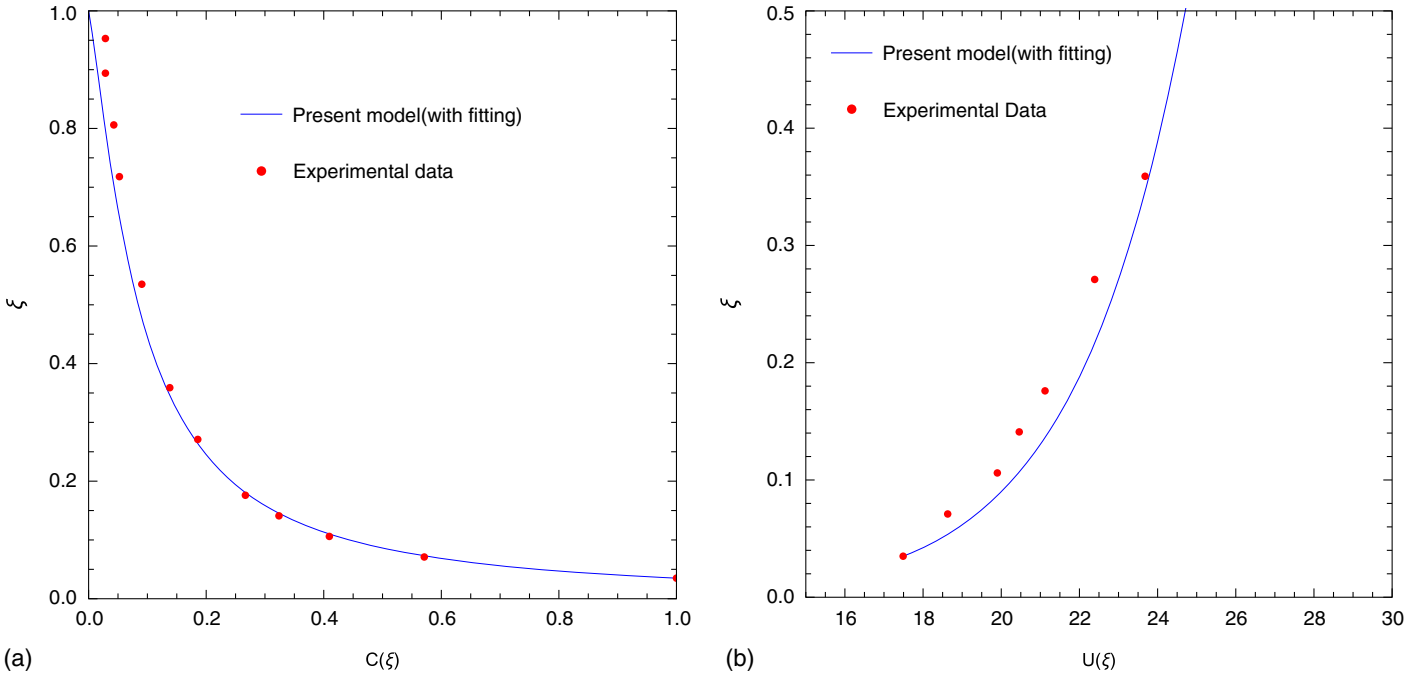

Fig. 11. Comparison of derived models with Run 23 of Coleman (1981): (a) concentration profile; and (b) velocity profile. Continuous line stands for the present model with α and β as fitting parameters, and the dots stand for the experimental data.

It can be observed from the figures that the models do not match the experimental data well when α and β are not fitted. On the other hand, if one parameter is fitted (α in Fig. 8 and β in Fig. 9) and other one is kept fixed (β in Fig. 8 and α in Fig. 9), then either velocity or concentration can be matched, but not both. Models are found to match best with the experimental data only when α and β both are taken as best-fitted parameters. A similar approach of fitting was also done by Herrmann and Madsen (2007). This may be due to the fact that the value of β taken to be equal to 4 in this work is not universal but rather may vary with data, and no expression of α is available in the literature that incorporates the stratification effect, including the work on α considered in the present study. Therefore, it may be natural that the velocity and concentration profiles are influenced by α and β together.

Apart from the aforementioned runs considering α and β as fitting parameters, the present models were validated with the experimental Runs 13 and 23 of Coleman (1981) and Runs S1 and S9 of Einstein and Chien (1955), as shown in Figs. 10–13. Required

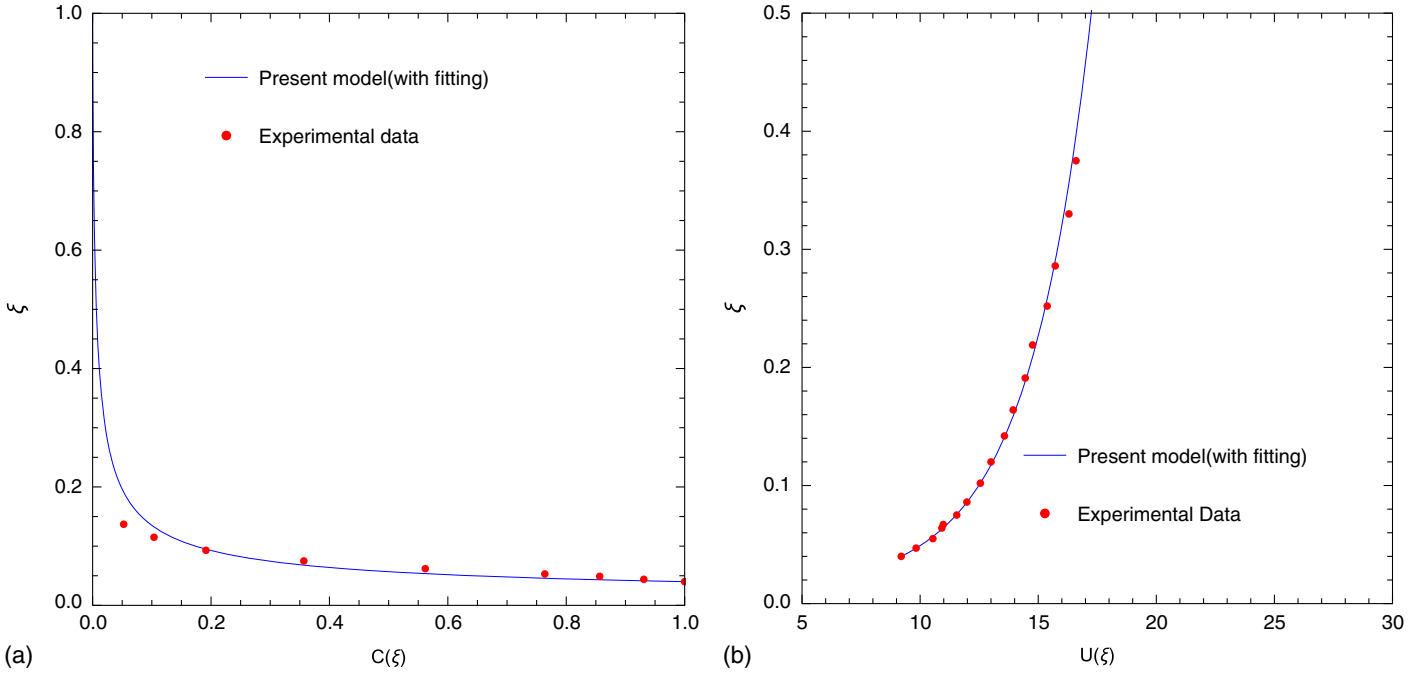

Fig. 12. Comparison of derived models with Run S1 of Einstein and Chien (1955): (a) concentration profile; and (b) velocity profile. Continuous line stands for the present model with α and β as fitting parameters, and the dots stand for the experimental data.

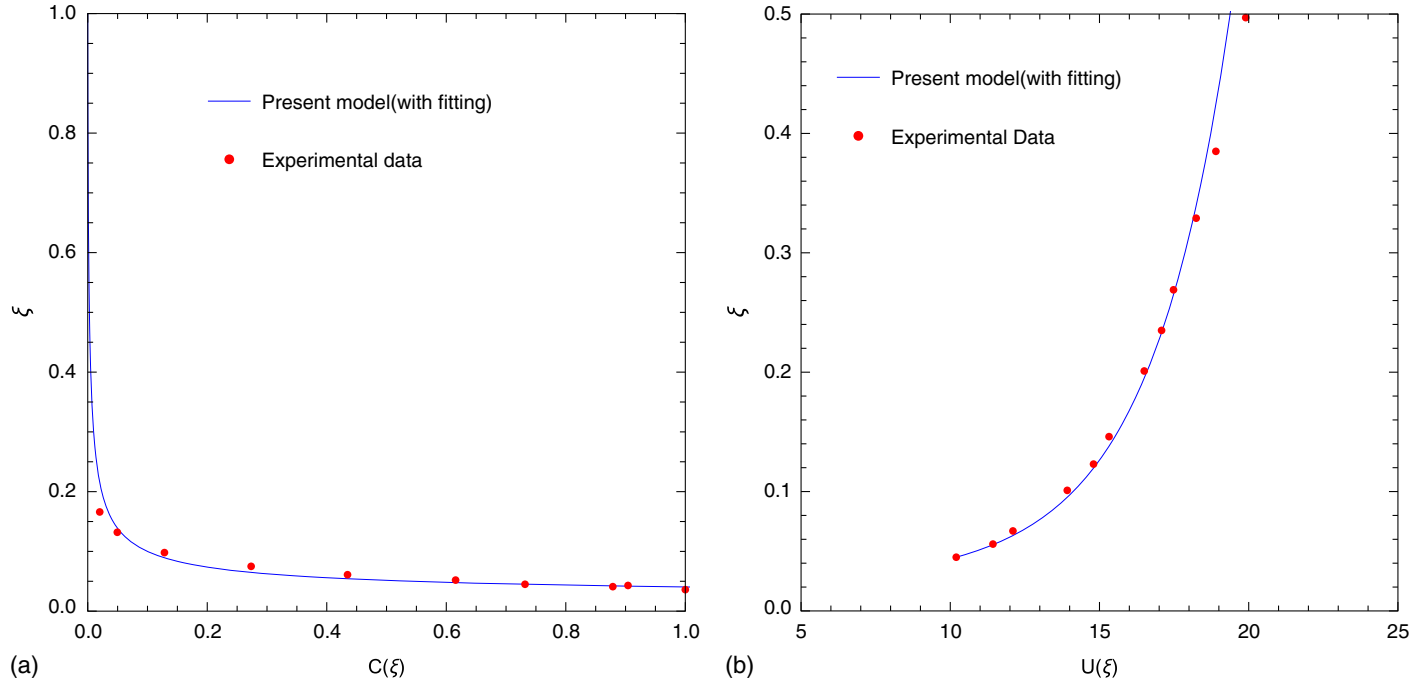

Fig. 13. Comparison of derived models with Run S9 of Einstein and Chien (1955): (a) concentration profile; and (b) velocity profile. Continuous line stands for the present model with α and β as fitting parameters, and the dots stand for the experimental data.

Table 2. Summary of experimental data

										α		β	
Data source	Run	ξ_a	c_a	$U(\xi=\xi_a)$	ω_0 (cm/s)	u_* (cm/s)	d (cm)	h (cm)	n_H	With fitting	Without fitting	With fitting	Without fitting
Coleman (1981)	13	0.035	0.0140	14.63	0.6623	4.10	0.0105	17.1	4.45	0.81	0.5512	6.25	4
	23	0.035	0.0021	17.49	2.0800	4.10	0.0210	17.0	3.79	1.85	2.0020	2.23	4
	35	0.035	0.00093	16.78	5.0545	4.10	0.0420	17.2	3.24	4.08	5.0367	3.05	4
Einstein	S1	0.040	0.02189	9.20	13.5146	11.47	0.130	13.8	2.62	2.29	1.2992	8.98	4
and Chien (1955)	S9	0.045	0.06528	10.20	10.6225	11.85	0.094	13.5	2.78	1.76	1.0824	14.58	4
	S12	0.030	0.07721	10.09	3.0201	10.09	0.0274	13.2	3.56	0.75	0.5056	8.96	4

parameters for assessing the models are reported in Table 2. It can be observed from the figures that the derived equations mimic the data well throughout the flow depth considered. As mentioned previously, the present model is applicable for nondilute flows also, and so it works well for the data of Einstein and Chien (1955).

Conclusions

The following conclusions can be drawn from the present work:

- This study modeled streamwise fluid velocity and suspended-sediment concentration distributions simultaneously along a vertical in a turbulent flow laden with sediment incorporating the effects of stratification and hindered settling, which is a generalization of the work of Herrmann and Madsen (2007). The theoretical formulation leads to a system of strongly nonlinear coupled odes, which has been solved to find an explicit series solution using HAM.
- In HAM, the convergence of the series depends on some auxiliary parameters, commonly called convergence control parameters. Those parameters monitor and control the convergency of the solutions. In the present study, three such parameters played this role, and they were determined through the averaged squared residual error of the system.
- The effects of stratification through stratification correction parameter (β), the hindered settling mechanism through the exponent of the reduction in settling velocity (n_H), and inverse Schmidt number (α) on the vertical distribution of velocity and concentration have been shown graphically as well as through discussion. It was found that the stratification effect leads to a decrease in concentration profile and increase in velocity profile compared with the neutral flow. On the other hand, as the inverse Schmidt number increases, the magnitude of velocity and concentration increase.
- The HAM-based approximate series solution has been validated with the numerical solution as well as with laboratory experimental data. Data for both dilute and nondilute flow have been considered, and the model shows good agreement with the observed values for both the cases when α and β are treated as fitting parameters. This finding is consistent with the results of Herrmann and Madsen (2007).
- Overall, the study has shown the potential of HAM in the context of dealing strong nonlinear problems in the area of sediment transport. Therefore, the applicability of the methodology in the

respective area is beyond doubt, and interested readers may extend it to explore other kinds of problems in this area.

Appendix I. Homotopy Derivative of General Function

Following Liao (2012), the proof of the closed form obtained in Eq. (45) is given in the following:

Theorem 1: Define an operator

$$\hat{\mathcal{D}}_m\Phi = \frac{1}{m!}\frac{\partial^m \Phi}{\partial q^m}$$

For a smooth function $f \in C^{\infty}(a, b)$ and a homotopy-Maclaurin series

$$\Phi = \sum_{k=0}^{\infty} \Phi_k q^k$$

it holds that

$$\hat{\mathcal{D}}_0[f(\Phi)] = f(\Phi) \tag{53}$$

$$\hat{\mathcal{D}}_m[f(\Phi)] = \sum_{k=0}^{m-1}\left(1-\frac{k}{m}\right)\hat{\mathcal{D}}_{m-k}(\Phi)\frac{\partial}{\partial\Phi}\{\hat{\mathcal{D}}_k[f(\Phi)]\} \tag{54}$$

and

$$\mathcal{D}_m[f(\Phi)] = \{\hat{\mathcal{D}}_m[f(\Phi)]\}|_{q=0} \tag{55}$$

Proof: It is easy to check that $\hat{\mathcal{D}}_0[f(\Phi)] = f(\Phi)$. In case of $m \geq 1$, applying Leibnitz's rule for derivative of the product, one obtains

$$\begin{aligned}\hat{\mathcal{D}}_m[f(\Phi)] &= \frac{1}{m!}\frac{\partial^m f(\Phi)}{\partial q^m} = \frac{1}{m!}\frac{\partial^{m-1}}{\partial q^{m-1}}\left[\frac{\partial\Phi}{\partial q}\frac{\partial f(\Phi)}{\partial q}\right]\\ &= \frac{1}{m!}\sum_{k=0}^{m-1}\frac{(m-1)!}{k!(m-1-k)!}\frac{\partial^{m-1-k}}{\partial q^{m-1-k}}\left(\frac{\partial\Phi}{\partial q}\right)\frac{\partial^k}{\partial q^m}\left[\frac{\partial f(\Phi)}{\partial\Phi}\right]\\ &= \sum_{k=0}^{m-1}\frac{m-k}{m}\left[\frac{1}{(m-k)!}\frac{\partial^{m-k}\Phi}{\partial q^{m-k}}\right]\left\{\frac{1}{k!}\frac{\partial^k}{\partial q^k}\left[\frac{\partial f(\Phi)}{\partial\Phi}\right]\right\}\\ &= \sum_{k=0}^{m-1}\left(1-\frac{k}{m}\right)\hat{\mathcal{D}}_{m-k}(\Phi)\hat{\mathcal{D}}_k\left[\frac{\partial f(\Phi)}{\partial\Phi}\right]\end{aligned} \tag{56}$$

Because $\hat{\mathcal{D}}_k[\partial f(\Phi)/\partial\Phi] = (\partial/\partial\Phi)\{\hat{\mathcal{D}}_k[f(\Phi)]\}$ holds, one can get

$$\hat{\mathcal{D}}_m[f(\Phi)] = \sum_{k=0}^{m-1}\left(1-\frac{k}{m}\right)\hat{\mathcal{D}}_{m-k}(\Phi)\frac{\partial}{\partial\Phi}\{\hat{\mathcal{D}}_k[f(\Phi)]\} \quad \text{for } m \geq 1$$

Then, according to the definition of $\hat{\mathcal{D}}_m$, it obviously holds that $\mathcal{D}_m[f(\Phi)] = \{\hat{\mathcal{D}}_m[f(\Phi)]\}|_{q=0}$.

Appendix II. Convergence Theorems

Recalling the theorems given in Liao (2012), the theoretical convergence analysis is done as follows:

Theorem 2: If the homotopy series $\sum_{m=0}^{\infty} y_{i,m}(\xi)$ and $\sum_{m=0}^{\infty} y'_{i,m}(\xi)$ converge, then $R_{i,m}(\vec{y}_{i,m-1})$ defined by the relation Eq. (30) satisfies $\sum_{m=1}^{\infty} R_{i,m}(\vec{y}_{i,m-1}) = 0$.

Proof: The auxiliary linear operator is defined as follows:

$$\mathcal{L}_i[y_i] = \xi\frac{dy_i}{d\xi} \tag{57}$$

According to Eq. (27), one obtains

$$\mathcal{L}_i[y_{i,1}] = h_i R_{i,1}(\vec{y}_{i,0}) \tag{58}$$

$$\mathcal{L}_i[y_{i,2} - y_{i,1}] = h_i R_{i,2}(\vec{y}_{i,1}) \tag{59}$$

$$\mathcal{L}_i[y_{i,3} - y_{i,2}] = h_i R_{i,3}(\vec{y}_{i,2}) \tag{60}$$

$$\vdots \tag{61}$$

$$\mathcal{L}_i[y_{i,m} - y_{i,m-1}] = h_i R_{i,m}(\vec{y}_{i,m-1}) \tag{62}$$

Adding all the preceding terms yields

$$\mathcal{L}_i[y_{i,m}] = h_i\sum_{k=1}^{m} R_{i,k}(\vec{y}_{i,k-1}) \tag{63}$$

Because the series $\sum_{m=0}^{\infty} y_{i,m}(\xi)$ and $\sum_{m=0}^{\infty} y'_{i,m}(\xi)$ converge, $\lim_{m\to\infty} y_{i,m}(\xi) = 0$ and $\lim_{m\to\infty} y'_{i,m}(\xi) = 0$. Now, recalling the aforementioned summand and taking the limit, the required result is

$$\begin{aligned}h_i\sum_{k=1}^{\infty} R_{i,k}(\vec{y}_{i,k-1}) &= \lim_{m\to\infty} h_i\sum_{k=1}^{m} R_{i,k}(\vec{y}_{i,k-1})\\ &= \lim_{m\to\infty}\mathcal{L}_i[y_{i,m}] = \lim_{m\to\infty}\xi y'_{i,m} = 0\end{aligned} \tag{64}$$

Theorem 3: As long as the series

$$y_i(\xi) = y_{i,0}(\xi) + \sum_{m=1}^{\infty} y_{i,m}(\xi)$$

converge, where the values of $y_{i,m}$ is governed by Eqs. (41) and (42), they must be solutions of original system of governing equations Eqs. (12) and (13).

Proof: From Theorem 2

$$\sum_{m=1}^{\infty} R_{i,m}(\vec{y}_{i,m-1}) = 0 \tag{65}$$

According to the definition of $R_{i,m}(\vec{y}_{i,m-1})$ given by Eq. (30)

$$\begin{aligned}\sum_{m=1}^{\infty} R_{i,m}(\vec{y}_{i,m-1}) &= \sum_{m=1}^{\infty}\frac{1}{(m-1)!}\frac{\partial^{m-1}\mathcal{N}_i[\Phi_i(\xi;q)]}{\partial q^{m-1}}\bigg|_{q=0}\\ &= \sum_{m=0}^{\infty}\frac{1}{m!}\frac{\partial^m\mathcal{N}_i[\Phi_i(\xi;q)]}{\partial q^m}\bigg|_{q=0}\end{aligned} \tag{66}$$

Suppose $\varepsilon_i(\xi;q) = \mathcal{N}_i[\Phi_i(\xi;q)]$ denotes the residual error of the system Eqs. (12) and (13). Clearly, $\varepsilon_i(\xi;q) = 0$ corresponds to the exact solutions of the original system of equations Eqs. (12) and (13). Now, expanding $\varepsilon_i(\xi;q)$ in Maclaurin's series about the embedding parameter q, one has

$$\varepsilon_i(\xi;q) = \sum_{m=0}^{\infty}\frac{q^m}{m!}\frac{\partial^m\varepsilon_i(\xi;q)}{\partial q^m}\bigg|_{q=0} = \sum_{m=0}^{\infty}\frac{q^m}{m!}\frac{\partial^m\mathcal{N}_i[\Phi_i(\xi;q)]}{\partial q^m}\bigg|_{q=0} \tag{67}$$

Using Eqs. (66) and (65), at $q = 1$, the preceding expression becomes

J. Eng. Mech., 2019, 145(11): 04019090

$$\varepsilon_i(\xi;1) = \sum_{m=0}^{\infty} \frac{1}{m!} \frac{\partial^m \mathcal{N}_i[\Phi_i(\xi;q)]}{\partial q^m}\bigg|_{q=0} = 0 \tag{68}$$

This means that the exact solutions of the original system of equations Eqs. (12) and (13) are obtained when $q = 1$. Therefore, as long as the series

$$y_i(\xi) = y_{i,0}(\xi) + \sum_{m=1}^{\infty} y_{i,m}(\xi)$$

converges, they must be the solutions of the original system of governing equations Eqs. (12) and (13).

Acknowledgments

The last two authors are thankful to the Science and Engineering Research Board (SERB), Department of Science and Technology (DST), Government of India for providing financial support through Research Project No. EMR/2015/002434. The authors are thankful to Professor Subhasish Dey (Department of Civil Engineering, IIT Kharagpur, India), the advisor of this project, for his valuable advice.

References

Abbasbandy, S. 2008. "Homotopy analysis method for generalized Benjamin-Bona-Mahony equation." *Zeitschrift für angewandte Mathematik und Physik* 59 (1): 51–62. https://doi.org/10.1007/s00033-007-6115-x.

Absi, R. 2011. "An ordinary differential equation for velocity distribution and dip-phenomenon in open channel flows." *J. Hydraul. Res.* 49 (1): 82–89. https://doi.org/10.1080/00221686.2010.535700.

Adomian, G. 2013. Vol. 60 of *Solving frontier problems of physics: The decomposition method*. New York: Springer.

Agnew, R. P. 1944. "Euler transformations." *Am. J. Math.* 66 (2): 313–338. https://doi.org/10.2307/2371990.

Cang, J., Y. Tan, H. Xu, and S.-J. Liao. 2009. "Series solutions of non-linear Riccati differential equations with fractional order." *Chaos Solitons Fractals* 40 (1): 1–9. https://doi.org/10.1016/j.chaos.2007.04.018.

Cheng, N.-S. 1997. "Simplified settling velocity formula for sediment particle." *J. Hydraul. Eng.* 123 (2): 149–152. https://doi.org/10.1061/(ASCE)0733-9429(1997)123:2(149).

Chien, N., and Z. Wan. 1999. *Mechanics of sediment transport*. Reston, VA: ASCE.

Coleman, N. L. 1970. "Flume studies of the sediment transfer coefficient." *Water Resour. Res.* 6 (3): 801–809. https://doi.org/10.1029/WR006i003p00801.

Coleman, N. L. 1981. "Velocity profiles with suspended sediment." *J. Hydraul. Res.* 19 (3): 211–229. https://doi.org/10.1080/00221688109499516.

Dey, S. 2014. *Fluvial hydrodynamics*. New York: Springer.

Einstein, H., and N. Chien. 1955. *Effects of heavy sediment concentration near the bed on velocity and sediment distribution*. MRD Sediment Series No. 8. Berkeley, CA: Univ. of California.

Garcia, M. H. 2008. "Sediment transport and morphodynamics." In *Sedimentation engineering: Processes, measurements, modeling, and practice*, 21–163. Reston, VA: ASCE.

Garside, J., and M. R. Al-Dibouni. 1977. "Velocity-voidage relationships for fluidization and sedimentation in solid-liquid systems." *Ind. Eng. Chem. Process Des. Dev.* 16 (2): 206–214. https://doi.org/10.1021/i260062a008.

Ghoshal, K., and S. Kundu. 2013. "Influence of secondary current on vertical concentration distribution in an open channel flow." *ISH J. Hydraul. Eng.* 19 (2): 88–96. https://doi.org/10.1080/09715010.2013.787714.

Ghoshal, K., and B. Mazumder. 2005. "Sediment-induced stratification in turbulent open-channel flow." *Environmetrics: Off. J. Int. Environmetrics Soc.* 16 (7): 673–686. https://doi.org/10.1002/env.729.

Graf, W., and M. Cellino. 2002. "Suspension flows in open channels; experimental study." *J. Hydraul. Res.* 40 (4): 435–447. https://doi.org/10.1080/00221680209499886.

Grasman, J. 2012. Vol. 63 of *Asymptotic methods for relaxation oscillations and applications*. New York: Springer.

Guo, J., and P. Y. Julien. 2002. "Modified log-wake law in smooth rectangular open-channels." In *Advances in hydraulics and water engineering: Volumes I & II*, 87–99. River Edge, NJ: World Scientific.

He, J.-H. 1999. "Homotopy perturbation technique." *Comput. Methods Appl. Mech. Eng.* 178 (3–4): 257–262. https://doi.org/10.1016/S0045-7825(99)00018-3.

Herrmann, M. J., and O. S. Madsen. 2007. "Effect of stratification due to suspended sand on velocity and concentration distribution in unidirectional flows." *J. Geophys. Res.: Oceans* 112 (C2): C02006. https://doi.org/10.1029/2006JC003569.

Huang, S.-H., Z.-L. Sun, D. Xu, and S.-S. Xia. 2008. "Vertical distribution of sediment concentration." *J. Zhejiang Univ.–Sci. A* 9 (11): 1560–1566. https://doi.org/10.1631/jzus.A0720106.

Hunt, J. 1954. "The turbulent transport of suspended sediment in open channels." *Proc. R. Soc. Lond. A* 224 (1158): 322–335. https://doi.org/10.1098/rspa.1954.0161.

Jing, H., G. Chen, W. Wang, and G. Li. 2018. "Effects of concentration-dependent settling velocity on non-equilibrium transport of suspended sediment." *Environ. Earth Sci.* 77 (15): 549. https://doi.org/10.1007/s12665-018-7731-9.

Jobson, H. E., and W. W. Sayre. 1970. "Vertical transfer in open channel flow." *J. Hydraul. Div.* 96 (3): 703–724.

Karmishin, A., A. Zhukov, and V. Kolosov. 1990. *Methods of dynamics calculation and testing for thin-walled structures*. Moscow: Mashinostroyenie.

Kumbhakar, M., J. Saha, K. Ghoshal, J. Kumar, and V. P. Singh. 2018. "Vertical sediment concentration distribution in high-concentrated flows: An analytical solution using homotopy analysis method." *Commun. Theor. Phys.* 70 (3): 367–378. https://doi.org/10.1088/0253-6102/70/3/367.

Kundu, S., and K. Ghoshal. 2012. "An analytical model for velocity distribution and dip-phenomenon in uniform open channel flows." *Int. J. Fluid Mech. Res.* 39 (5): 381–395. https://doi.org/10.1615/InterJFluidMechRes.v39.i5.20.

Lagerstrom, P. A. 2013. Vol. 76 of *Matched asymptotic expansions: Ideas and techniques*. New York: Springer.

Lane, E., and A. Kalinske. 1941. "Engineering calculations of suspended sediment." *Eos Trans. Am. Geophys. Union* 22 (3): 603–607. https://doi.org/10.1029/TR022i003p00603.

Lassabatere, L., J. H. Pu, H. Bonakdari, C. Joannis, and F. Larrarte. 2012. "Velocity distribution in open channel flows: Analytical approach for the outer region." *J. Hydraul. Eng.* 139 (1): 37–43. https://doi.org/10.1061/(ASCE)HY.1943-7900.0000609.

Lavelle, J., and W. Thacker. 1978. "Effects of hindered settling on sediment concentration profiles." *J. Hydraul. Res.* 16 (4): 347–355. https://doi.org/10.1080/00221687809499612.

Liao, S. 2003. *Beyond perturbation: Introduction to the homotopy analysis method*. Boca Raton, FL: CRC Press.

Liao, S. 2012. *Homotopy analysis method in nonlinear differential equations*. New York: Springer.

Liao, S. J. 1992. "The proposed homotopy analysis technique for the solution of nonlinear problems." Ph.D. thesis, School of Naval Architecture and Ocean Engineering, Shanghai Jiao Tong Univ.

Liao, S.-J. 1999a. "An explicit, totally analytic approximate solution for Blasius' viscous flow problems." *Int. J. Non-Linear Mech.* 34 (4): 759–778. https://doi.org/10.1016/S0020-7462(98)00056-0.

Liao, S.-J. 1999b. "A uniformly valid analytic solution of two-dimensional viscous flow over a semi-infinite flat plate." *J. Fluid Mech.* 385 (Apr): 101–128. https://doi.org/10.1017/S0022112099004292.

Liao, S.-J., and K. F. Cheung. 2003. "Homotopy analysis of nonlinear progressive waves in deep water." *J. Eng. Math.* 45 (2): 105–116. https://doi.org/10.1023/A:1022189509293.

Liu, Z., and S.-J. Liao. 2014. "Steady-state resonance of multiple wave interactions in deep water." *J. Fluid Mech.* 742 (Mar): 664–700. https://doi.org/10.1017/jfm.2014.2.
Lu, J., Y. Zhou, Y. Zhu, J. Xia, and L. Wei. 2018. "Improved formulae of velocity distributions along the vertical and transverse directions in natural rivers with the sidewall effect." *Environ. Fluid Mech.* 18 (6): 1491–1508. https://doi.org/10.1080/00207179208934253.
Lyapunov, A. M. 1992. "The general problem of the stability of motion." *Int. J. Control* 55 (3): 531–534. https://doi.org/10.1080/00207179208934253.
Majumdar, H., and M. R. Carstens. 1967. *Diffusion of particles by turbulence: Effect of particle size*. Georgia Institute of Technology Rep. No. WRC-0967. St. Paul, MN: Water Resources Center.
Massa, F., T. Tison, B. Lallemand, and O. Cazier. 2011. "Structural modal reanalysis methods using homotopy perturbation and projection techniques." *Comput. Methods Appl. Mech. Eng.* 200 (45–46): 2971–2982. https://doi.org/10.1016/j.cma.2011.06.016.
Maude, A., and R. Whitmore. 1958. "A generalized theory of sedimentation." *Br. J. Appl. Phys.* 9 (12): 477–482. https://doi.org/10.1088/0508-3443/9/12/304.
Mazumder, B., and K. Ghoshal. 2002. "Velocity and suspension concentration in sediment-mixed fluid." *Int. J. Sediment Res.* 17 (3): 220–232.
Monin, A., and A. Yaglom. 1971. Vol. I of *Statistical fluid dynamics*. Cambridge, MA: MIT Press.
Nayfeh, A. H. 2011. *Introduction to perturbation techniques*. New York: Wiley.
Pal, D., and K. Ghoshal. 2013. "Hindered settling with an apparent particle diameter concept." *Adv. Water Resour.* 60 (Oct): 178–187. https://doi.org/10.1016/j.advwatres.2013.08.003.
Pal, D., and K. Ghoshal. 2016a. "Effect of particle concentration on sediment and turbulent diffusion coefficients in open-channel turbulent flow." *Environ. Earth Sci.* 75 (18): 1245. https://doi.org/10.1007/s12665-016-6045-z.
Pal, D., and K. Ghoshal. 2016b. "Vertical distribution of fluid velocity and suspended sediment in open channel turbulent flow." *Fluid Dyn. Res.* 48 (3): 035501. https://doi.org/10.1088/0169-5983/48/3/035501.
Pal, D., and K. Ghoshal. 2017. "Hydrodynamic interaction in suspended sediment distribution of open channel turbulent flow." *Appl. Math. Modell.* 49 (Sep): 630–646. https://doi.org/10.1016/j.apm.2017.02.045.
Prandtl, L. 1932. "Zur turbulenten strömung in rohren und längs platten." *Ergeb. Aerodyn. Versuch. Series* 4: 18–29.
Richarson, J., and W. Zaki. 1954. "Sedimentation and fluidisation, part 1." *Trans. Ins. Chem. Eng.* 31: 35–53.
Rijn, L. C. V. 1984. "Sediment transport, Part II: Suspended load transport." *J. Hydraul. Eng.* 110 (11): 1613–1641. https://doi.org/10.1061/(ASCE)0733-9429(1984)110:11(1613).
Rouse, H. 1937. "Modern conceptions of the mechanics of fluid turbulence." *Trans. ASCE* 102 (1): 463–505.
Singh, M. K., A. Chatterjee, and V. P. Singh. 2017. "Solution of one-dimensional time fractional advection dispersion equation by homotopy analysis method." *J. Eng. Mech.* 143 (9): 04017103. https://doi.org/10.1061/(ASCE)EM.1943-7889.0001318.
Smith, J. D. 1975. *Modeling of sediment transport on continental shelves*. Rep. No. RLO-2225-T25-15. Seattle: Univ. of Washington.
Smith, J. D., and S. McLean. 1977a. "Boundary layer adjustments to bottom topography and suspended sediment." *Elsevier Oceanogr. Ser.* 19: 123–151. https://doi.org/10.1016/S0422-9894(08)70839-0.
Smith, J. D., and S. McLean. 1977b. "Spatially averaged flow over a wavy surface." *J. Geophys. Res.* 82 (12): 1735–1746. https://doi.org/10.1029/JC082i012p01735.
Thacker, W., and J. Lavelle. 1977. "Two-phase flow analysis of hindered settling." *Phys. Fluids* 20 (9): 1577–1579. https://doi.org/10.1063/1.862026.
Tsai, C.-H., and C.-T. Tsai. 2000. "Velocity and concentration distributions of sediment-laden open channel flow 1." *JAWRA J. Am. Water Resour. Assoc.* 36 (5): 1075–1086. https://doi.org/10.1111/j.1752-1688.2000.tb05711.x.
Umeyaina, M. 1992. "Vertical distribution of suspended sediment in uniform open-channel flow." *J. Hydraul. Eng.* 118 (6): 936–941. https://doi.org/10.1061/(ASCE)0733-9429(1992)118:6(936).
Umeyama, M., and F. Gerritsen. 1992. "Velocity distribution in uniform sediment-laden flow." *J. Hydraul. Eng.* 118 (2): 229–245. https://doi.org/10.1061/(ASCE)0733-9429(1992)118:2(229).
Vajravelu, K., K. Prasad, J. Lee, C. Lee, I. Pop, and R. A. Van Gorder. 2011. "Convective heat transfer in the flow of viscous ag-water and cu-water nanofluids over a stretching surface." *Int. J. Therm. Sci.* 50 (5): 843–851. https://doi.org/10.1016/j.ijthermalsci.2011.01.008.
Van Gorder, R. A. 2012. "Control of error in the homotopy analysis of semi-linear elliptic boundary value problems." *Numer. Algorithms* 61 (4): 613–629. https://doi.org/10.1007/s11075-012-9554-1.
Villaret, C., and J. Trowbridge. 1991. "Effects of stratification by suspended sediments on turbulent shear flows." *J. Geophys. Res.: Oceans* 96 (C6): 10659–10680. https://doi.org/10.1029/91JC01025.
Winterwerp, J. C., M. B. de Groot, D. R. Mastbergen, and H. Verwoert. 1990. "Hyperconcentrated sand-water mixture flows over a flat bed." *J. Hydraul. Eng.* 116 (1): 36–54. https://doi.org/10.1061/(ASCE)0733-9429(1990)116:1(36).
Woo, H., P. Julien, and E. Richardson. 1988. "Suspension of large concentrations of sands." *J. Hydraul. Eng.* 114 (8): 888–898. https://doi.org/10.1061/(ASCE)0733-9429(1988)114:8(888).
Wright, S., and G. Parker. 2004. "Flow resistance and suspended load in sand-bed rivers: Simplified stratification model." *J. Hydraul. Eng.* 130 (8): 796–805. https://doi.org/10.1061/(ASCE)0733-9429(2004)130:8(796).
Zhong, X., and S. Liao. 2018. "On the limiting Stokes wave of extreme height in arbitrary water depth." *J. Fluid Mech.* 843 (May): 653–679. https://doi.org/10.1017/jfm.2018.171.